PERGAMON

International Journal of Solids and Structures 36 (1999) 4869–4888

INTERNATIONAL JOURNAL OF SOLIDS and STRUCTURES

A comparison between a semi-analytical and a numerical solution of a two-dimensional hydraulic fracture

R. Carbonell[a], Jean Desroches[b], Emmanuel Detournay[c,*]

[a] *Intevep S.A., Venezuela*
[b] *Schlumberger Well Services, U.S.A.*
[c] *Department of Civil Engineering, University of Minnesota, 500 Pillsbury Drive SE, Minneapolis, MN 55455, U.S.A.*

Received 2 September 1997; accepted 11 May 1998

Abstract

This paper compares a semi-analytical self-similar solution of the problem of a hydraulically driven fracture with results obtained using the numerical model Loramec. The problem under consideration is a hydraulic fracture propagating in an infinite impermeable elastic medium under plane strain conditions. The fracture is driven by an incompressible Newtonian fluid injected, at a constant rate, from a source located at the center of the fracture. There are some differences between the two models in regard to the modeling of the near tip processes. The semi-analytical solution is built on the assumptions that the fracture is completely filled by the injection fluid and that the solid has zero toughness, while the numerical model explicitly accounts for the existence of a priori unknown lag between the fluid and crack front. It is shown that the numerical results exhibit self-similarity; in particular the predicted power law dependence on time of the net pressure, aperture and fracture length is well observed in the numerical results. Also, a very good agreement between the self-similar and the numerical solution is observed under conditions of 'small' toughness. The results of this study actually suggest that the self-similar zero toughness solution is a good approximation to cases where the rock has a non-zero fracture toughness and a fluid lag develops, provided that the ratio θ of the rate of energy dissipation in the solid over the viscous dissipation in the fluid is less than 10^{-2}.

Nomenclature

$\mathscr{D}$ dimensionless viscous dissipation
E' plane strain modulus
$\mathscr{G}$ dimensionless energy release rate
K_{Ic} toughness
$\mathscr{K}$ dimensionless toughness

* Corresponding author. Tel.: 001 612 625 3043; fax: 001 612 626 7750; e-mail: detou001@maroon.tc.umn.edu

0020-7683/99/$ - see front matter
PII: S0020-7683(98)00269-8

L characteristic length
l half-fracture length (length of one wing)
p net pressure
p_f fluid pressure
q flow rate
Q_o constant injection rate
T characteristic time
t time
x space coordinate with origin at the center of the fracture
w crack opening.

Greek symbols
γ volumetric constant
θ solid to fluid dissipation ratio
λ dimensionless fracture length
μ fluid viscosity
ξ dimensionless coordinate (similarity variable)
Π dimensionless net pressure
σ_o far-field minimum principal stress
τ dimensionless time
Ψ dimensionless flow rate
Ω dimensionless crack opening.

1. Introduction

Hydraulic fracturing is one of the most important stimulation techniques of the energy industry. This operation is used to enhance the flow of fluids from oil, gas and geothermal reservoirs. Mathematical modeling of the hydraulic fracturing process is performed in order to predict the fracture response to both reservoir and fluid properties, in situ stresses and pumping rate (Perkins and Kern, 1961; Nordgren, 1972; Geerstma and Haafkens, 1979; Nilson, 1988). Challenging difficulties in modeling arise from the non-local character of the response of the fracture and the highly non-linear coupling between the equations governing fluid flow in the fracture and those which govern rock deformation produced by fluid pressure. This problem persists even if, as in this paper, one restricts oneself to the framework of linear elasticity and lubrication theory.

In this paper, we compare a semi-analytical solution (computable to any required level of accuracy) of the problem of a hydraulically driven fracture (Carbonell, 1996; Carbonell and Detournay, 1998), with results obtained with the numerical code Loramec (Desroches and Thiercelin, 1993). The semi-analytical solution is built on the restrictive assumptions of a zero toughness solid and zero lag between the fluid and crack front. Also, this solution makes use of recent results obtained by the SCR Geomechanics Group (Desroches et al., 1994) regarding the asymptotic behavior of the solution near the fracture tip. This near tip solution corresponds to an exact matching singularity between the lubrication and the elasticity equations, which differs from the classical results of linear elastic fracture mechanics.

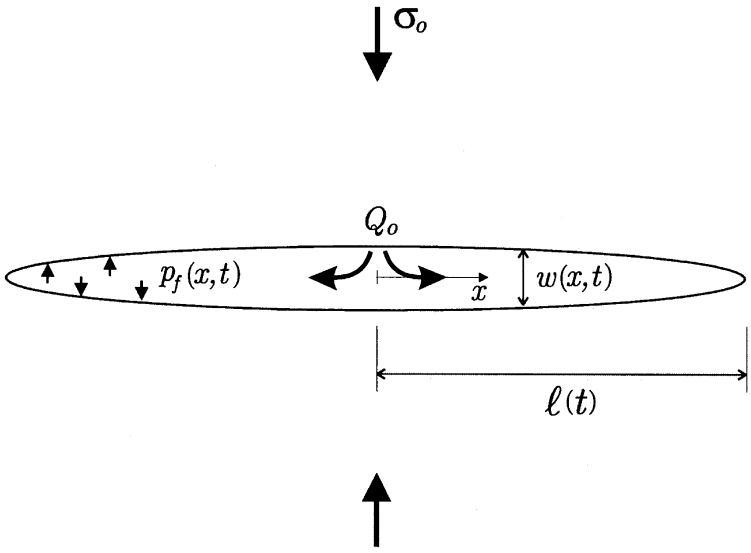

Fig. 1. Two-dimensional fluid-driven fracture.

The problem under consideration is a hydraulic fracture propagating in an infinite impermeable elastic medium under plane strain conditions, see Fig. 1. A far-field compressive stress of magnitude σ_o acts perpendicular to the fracture. The fracture is driven by an incompressible Newtonian fluid injected from a source located at the center of the fracture. It is assumed that the fracture is in mobile equilibrium at all time, and that crack propagation is quasi-static. Also, the flow of fluid in the fracture is modelled using the lubrication approximation.

Given that fluid is injected into the fracture at a constant volumetric flow rate Q_o, we seek to determine the fracture half-length l as a function of time t, the crack opening w, and the fluid pressure p_f (or the net pressure $p = p_f - \sigma_o$) as a function of both position (defined by the coordinate x with origin at the center of the fracture) and time t.

The main objective of this comparative study is to evaluate the relevance of the zero toughness solution to predict the characteristics of a hydraulic fracture propagating in a rock of finite toughness.

2. Self-similar formulation

A self-similar solution for the considered hydraulic fracture problem has recently been obtained by Carbonell and Detournay (1998). This solution (hereafter referred to as CD) is based, however, on two additional assumptions: (1) the fracture is completely filled by the injected fluid (in other words, the fluid front coincides with the crack tip); (2) the solid has a zero fracture toughness. In the following, we outline the mathematical basis of the CD solution. It is worthwhile to note that a self-similar solution for the case of zero toughness can be obtained for an injection rate varying either as a power law or an exponential function of time (Spence and Sharp, 1985), although here we restrict considerations to a constant injection rate Q_o.

2.1. Governing equations

The theory of elasticity provides a relation between the net pressure $p(x, t) = p_f(x, t) - \sigma_o$ and crack width $w(x, t)$ (Rice, 1968)

$$p = \frac{E'}{4\pi} \int_{-l}^{l} \frac{\partial w(s,t)}{\partial s} \frac{\mathrm{d}s}{x-s} \tag{1}$$

where $E' = E/(1-\nu^2)$ is the plane strain modulus written in terms of Young's modulus E and Poisson's ratio ν.

The lubrication equation, or Reynolds equation, that governs the flow of fluid in the fracture is given by (Batchelor, 1967)

$$\frac{\partial w}{\partial t} = \frac{1}{12\mu} \frac{\partial}{\partial x} \left(w^3 \frac{\partial p}{\partial x} \right). \tag{2}$$

This equation is obtained by combining the continuity equation with Poiseuille law

$$\frac{\partial w}{\partial t} + \frac{\partial q}{\partial x} = 0 \quad q = -\frac{w^3}{12\mu} \frac{\partial p}{\partial x} \tag{3}$$

where q denotes the volumetric flow rate, and μ the fluid viscosity.

2.2. Initial and boundary conditions

In view of the symmetry of the problem with respect to the position of the source (which corresponds to the origin of the coordinate, $x = 0$), the inlet flow boundary condition translates into

$$q|_{x=0^+} = -q|_{x=0^-} = \frac{Q_o}{2} \quad \text{at } x = 0. \tag{4}$$

The conditions at the fracture tips ($x = \pm l$) correspond to a zero crack opening and to no-flow

$$w = 0 \quad q = 0 \quad \text{at } x = \pm l. \tag{5}$$

This latter condition can also be translated into a condition on w and p, in view of eqn (3)

$$w^3 \frac{\mathrm{d}p}{\mathrm{d}x} = 0 \quad \text{at } x = \pm l. \tag{6}$$

Due to the symmetry in loading and geometry, the hydraulic fracture propagates solely in Mode I. The assumptions that the fracture is in mobile equilibrium at all times and that the rock has zero fracture toughness imply that the Mode I stress intensity factor K_I is equal to zero. The stress field ahead of the fracture tip does not exhibit, therefore, a square root singularity; rather, the following condition must be satisfied (Rice, 1968):

$$(l \mp x)^{-1/2} w = 0 \quad \text{at } x = \pm l. \tag{7}$$

Recent investigations of the near tip process have led to the obtention of an exact matching

singularity between the lubrication and the elasticity equations, under the conditions that the fluid front coincides with the crack tip and that the solid has zero toughness. For a Newtonian viscous fluid, the near-tip singular solutions for the net pressure p_* and the crack opening w_* are (Desroches et al., 1994)

$$\frac{w_*}{L_h} = 2^{1/3}3^{5/6}\xi_*^{2/3} \quad \frac{p_*}{E'} = -\frac{1}{2^{2/3}3^{2/3}\xi_*^{1/3}} \tag{8}$$

where the dimensionless coordinate ξ_* and the lengthscale L_h are defined as $\xi_* = (x-l)/L_h$ and $L_h = 12\,\mu\dot{l}/E'$. It is important to note that all the tip conditions (5), (6) and (7) are automatically satisfied with the asymptotic solution (8).

Finally, an alternative way to express the inlet flow boundary condition (4) is to equate the total injected volume of fluid $V(t)$ to the volume of the hydraulic fracture

$$V = \int_{-l}^{l} w\,\mathrm{d}s = Q_o t. \tag{9}$$

2.3. Dimensional considerations and similarity formulation

We first introduce a time scale T and a length scale L. Here, T is expressed in terms of the ratio of the fluid viscosity over the plane strain modulus, while L is introduced through the volume of fluid V injected during this characteristic time T

$$T = \frac{12\mu}{E'} \quad L = \sqrt{Q_o T}. \tag{10}$$

A dimensionless moving coordinate ξ and a dimensionless time τ are then defined as follows

$$\xi = \frac{x}{l} \quad \tau = \frac{t}{T}. \tag{11}$$

We now introduce the scaled fracture length $\chi(\tau)$ and the following dimensionless field quantities: the net pressure $\Pi(\xi,\tau)$, the flow rate $\Psi(\xi,\tau)$, and the crack aperture $\Omega(\xi,\tau)$

$$\chi = \frac{l}{L} \quad \Pi = \frac{p}{E'} \quad \Psi = \frac{qT}{L^2} \quad \Omega = \frac{w}{L}. \tag{12}$$

After conversion of variable from the fixed coordinate x to the moving coordinate ξ, the governing equations of the two-dimensional hydraulic fracture problem become

$$\Pi = -\frac{1}{4\pi\chi}\int_{-1}^{1}\frac{\partial\Omega}{\partial\rho}\frac{\mathrm{d}\rho}{\rho-\xi} \qquad \frac{\partial\Omega}{\partial\tau} - \xi\frac{\dot{\chi}}{\chi}\frac{\partial\Omega}{\partial\xi} = \frac{1}{\chi^2}\frac{\partial}{\partial\xi}\left(\Omega^3\frac{\partial\Pi}{\partial\xi}\right). \tag{13}$$

Following Spence and Sharp (1985), we now search for self-similar solutions for pressure and crack opening of the form

$$\Omega(\xi,\tau) = \gamma\tau^{1/3}\Omega_\xi(\xi) \quad \Pi(\xi,\tau) = \tau^{-1/3}\Pi_\xi(\xi) \tag{14}$$

as well as a power law expression for the scaled length $\chi(\tau)$

$$\chi(\tau) = \gamma\tau^{2/3} \tag{15}$$

where the a priori unknown constant γ is defined in terms of the fracture volume

$$\gamma^{-2} = \int_{-1}^{1} \Omega_\xi(\rho)\,\mathrm{d}\rho. \tag{16}$$

Substituting the above expressions in the governing eqns (13) yields a system of integro-differential equations

$$\Pi_\xi = -\frac{1}{4\pi}\int_{-1}^{1} \frac{\Omega'_\xi\,\mathrm{d}\rho}{\rho-\xi} \tag{17}$$

$$\frac{1}{3}\Omega_\xi - \frac{2}{3}\xi\Omega'_\xi = \frac{\mathrm{d}}{\mathrm{d}\xi}(\Omega_\xi^3\Pi'_\xi) \tag{18}$$

(with the prime denoting differentiation) subject to the following tip conditions

$$(1 \mp \xi)^{-1/2}\Omega_\xi = 0 \quad \Omega_\xi = 0 \quad \Omega_\xi^3\Pi'_\xi = 0 \quad \text{at } \xi = \pm 1. \tag{19}$$

It can readily be deduced from the Poiseuille eqn (3) and the above equations that the dimensionless flow rate Ψ does not depend on τ, and also can be written as

$$\Psi = \gamma^2\Psi_\xi(\xi) = -\gamma^2\Omega_\xi^3\Pi'_\xi. \tag{20}$$

Finally, by using the scaling eqns (11) and (12), the tip solution (8) can be recast into an asymptotic solution of the two functions $\Omega(\xi,\tau)$ and $\Pi(\xi,\tau)$ near the end points, $\xi = \pm 1$. Then, adopting the power law (15) for the fracture length, the near tip solution becomes

$$\Omega_\xi = 2^{2/3}3^{1/2}(1 \mp \xi)^{2/3} \quad \Pi_\xi = -\frac{1}{2^{1/3}3(1 \mp \xi)^{1/3}} \quad \text{for } |\xi \pm 1| \ll 1. \tag{21}$$

2.4. Method of solution

Determination of the net pressure $\Pi_\xi(\xi)$ and crack opening $\Omega_\xi(\xi)$ is carried out using a numerical method, inspired by the procedure described by Spence and Sharp (1985). This method consists in first finding a representation for Π_ξ and Ω_ξ, such that the elasticity eqn (17) and boundary conditions (19) are automatically satisfied. Furthermore, the solution F (i.e. either Π_ξ or Ω_ξ) is expressed as a sum of a 'general' and a 'particular' source solution, denoted as F^* and F^{**}, respectively

$$F(\xi) = F^*(\xi) + BF^{**}(\xi) \tag{22}$$

where B is a coefficient. On the one hand, the general solution F^* has the expected behavior at the fracture tips but is characterized by a zero pressure gradient at the source $\xi = 0$ (and therefore does not fulfill the expected behavior near the source eqn (4)). On the other hand, the particular solution F^{**} is characterized by a jump of the pressure gradient at $\xi = 0$ and by a non-singular behavior at the fracture tips. Finally, the general solution F^* is represented as an infinite series of base functions $F_i^*(\xi)$, i.e.

$$F^*(\xi) = \sum_{i=1}^{\infty} A_i F_i^*(\xi)$$

where A_i, $i = 1, \ldots, \infty$ are initially unknown coefficients, like B (see expressions for Π_ξ and Ω_ξ in appendix A).

In the CD solution, the base functions F_i^* are expressed in terms of Jacobi polynomials, rather than Chebyshev polynomials as done by Spence and Sharp (1985) who searched for a solution based on the LEFM square root singularity. Then, truncating the infinite series F^*, an n-order approximation $F^{(n)}(\xi)$ for pressure and crack opening is obtained. Substituting $F^{(n)}(\xi)$ into the lubrication equation leads to the formulation of a non-linear algebraic equation in ξ, containing the $(n+1)$ unknown coefficients. These $(n+1)$ free parameters are then computed by enforcing satisfaction of the non-linear algebraic equation at a set of $(n+1)$ collocation points ξ_j, $j = 1 \ldots n+1$, see Appendix A. Note that calculation of the coefficients carry not only an insignificant cost (of the order of 1 min on PC Pentium computer for $n = 10$), but that it needs to be performed only once.

The quantities γ, $\Pi_\xi(0)$, $\Omega_\xi(0)$ characterizing the solution are estimated to be $\gamma \simeq 0.613$, $\Pi_\xi(0) \simeq 0.546$, $\Omega_\xi(0) \simeq 1.839$, according to the approximation $n = 10$.

3. Numerical model

A detailed description of the numerical code Loramec is given by Desroches and Thiercelin (1993) and Desroches (1998). The code can be used to simulate the propagation of either plane strain or penny-shaped hydraulic fractures under very general conditions, such as variable injection rate, 'power-law' rheological behavior of the fluid (which includes Newtonian behavior), diffusion of fluid through the fracture walls. Although Loramec is not the most used model in the industry, it is the only hydraulic fracturing model the authors are aware of which compare well with carefully monitored laboratory data (Desroches and Thiercelin, 1993). Furthermore, Loramec is geared towards precision and focuses on what happens near the tip of the fracture, whereas most models in the industry are designed for speed and the prediction of overall quantities. A description of the model relevant to the cases investigated in this paper is presented in Appendix B.

The essential differences in the assumptions on which the two solutions are built concern the modeling of the tip process. In Loramec, the fracturing fluid does not necessarily reach the tip of the fracture; a fluid lag may develop. The pressure in the lag is taken either as the pore pressure for permeable rocks or as the fracturing fluid vapor pressure for impermeable rocks. If there is a lag, the pressure in the lag is known, and the lag size is unknown. If there is no fluid lag, however, the pressure at the tip is one of the unknowns. Finally, the propagation criterion in Loramec requires a non-zero fracture toughness, which can be 'small', however.

4. Comparison

4.1. Numerical simulations

In designing the comparative study, the input data of the simulations have been chosen in accordance with expected parameters for a hydraulic stimulation carried out in the field. The input

data used in the numerical simulations are: $Q_o = 4 \times 10^{-3}\,m^2\,s^{-1}$, $\nu = 0.15$, $\sigma_o = 50\,MPa$, $\mu = 853\,cp$ ($8.53 \times 10^{-7}\,MPa\,s^{-1}$), $E = 25\,GPa$, and $K_{Ic} = 0.001, 0.1, 1, 5$ and $10\,MPa\,m^{-1/2}$. The corresponding values of E', T, and L are: $E' = 25.6$ GPa, $T = 4 \times 10^{-10}$ s and $L = 1.265 \times 10^{-6}$ m. Also, we introduce the dimensionless toughness $\mathscr{K}$ defined as

$$\mathscr{K} = \frac{K_{Ic}}{E' L^{1/2}}. \tag{23}$$

Hence, the values for the dimensionless toughness used in the numerical simulations are: $\mathscr{K} = 3.5 \times 10^{-5}$, 3.5×10^{-3}, 3.5×10^{-2}, 1.7×10^{-1} and 3.5×10^{-1}.

Some of the specifics of the numerical calculations are given below. The computational grid consisted of 43 nodes, most of them being concentrated near the tip of the fracture. The computations started at 0.159 s and ended at 1000 s. The calculations took 296 time steps, with an average of 60 iterations per time step to converge onto the solution. Over the considered time interval, the fracture grew from an initial length of 0.4 m to a final length of 137 m, with the fracture length incrementally increased by 2% at each time step. The running time for one simulation was about 25 min on a Sun UltraSparc 1 workstation.

4.2. Results

Comparison of crack length $\lambda(\tau)$, pressure $\Pi(0,\tau)$, and fracture opening $\Omega(0,\tau)$ at the fluid injection point in terms of τ are shown in Fig. 2 for all values of toughness considered. Interestingly, the numerical results indicate a power law dependence on time, which is virtually identical to the self-similar solution. These results suggest that the numerical solution follows a self-similar pattern, at least for the set of parameters considered. It follows therefore that it is appropriate to compute from the raw numerical results the 'reduced' fracture opening Ω_ξ and net pressure Π_ξ according to eqn (14), and to compare these reduced results with the semi-analytical solution.

Comparison between the numerical and semi-analytical solution for toughness $\mathscr{K}$ up to 1.7×10^{-1} shows an excellent agreement between the two solutions. Representative results for $\Pi_\xi(\xi)$ and $\Omega_\xi(\xi)$ computed at different times are shown in Figs 3–5 for the cases $\mathscr{K} = 3.5 \times 10^{-5}$, 3.5×10^{-2} and 1.7×10^{-1}. However, plot (c) in Figs 3 and 4 for $\mathscr{K} < 10^{-2}$ shows a discrepancy between the two solutions near the tip at early time due to the presence of the fluid lag. (The fluid lag decreases in absolute terms with time.) These results suggest that the semi-analytical solution is capable of capturing the global behavior despite the fact that a fluid lag is present at the fracture tip. The numerical results also indicate that $\Omega_\xi(\xi)$ behaves as $(1-\xi)^{2/3}$ at an intermediate scale (see, for example plot (c) in Fig. 5). In other words, the simulations show evidence that eqn (8) develops as an intermediate asymptotics for these values of $\mathscr{K}$.

The results for the $\mathscr{K} = 3.5 \times 10^{-1}$ simulation are plotted in Fig. 6. The numerical results show a clear discrepancy with the semi-analytical solution. At the tip (see plot (c) in Fig. 6), the numerical results are characterized by $\Omega_\xi(\xi)$ behaving as $(1-\xi)^{1/2}$ near the tip and at an intermediate scale at all times. Hence for this particular simulation, the CD solution no longer applies, although the toughness is only twice the value corresponding to Fig. 6. These results imply not only the existence of a different solution for 'high toughness', but also a very rapid transition between two solutions. The excellent agreement observed between the CD solution and the numerical results, for the set

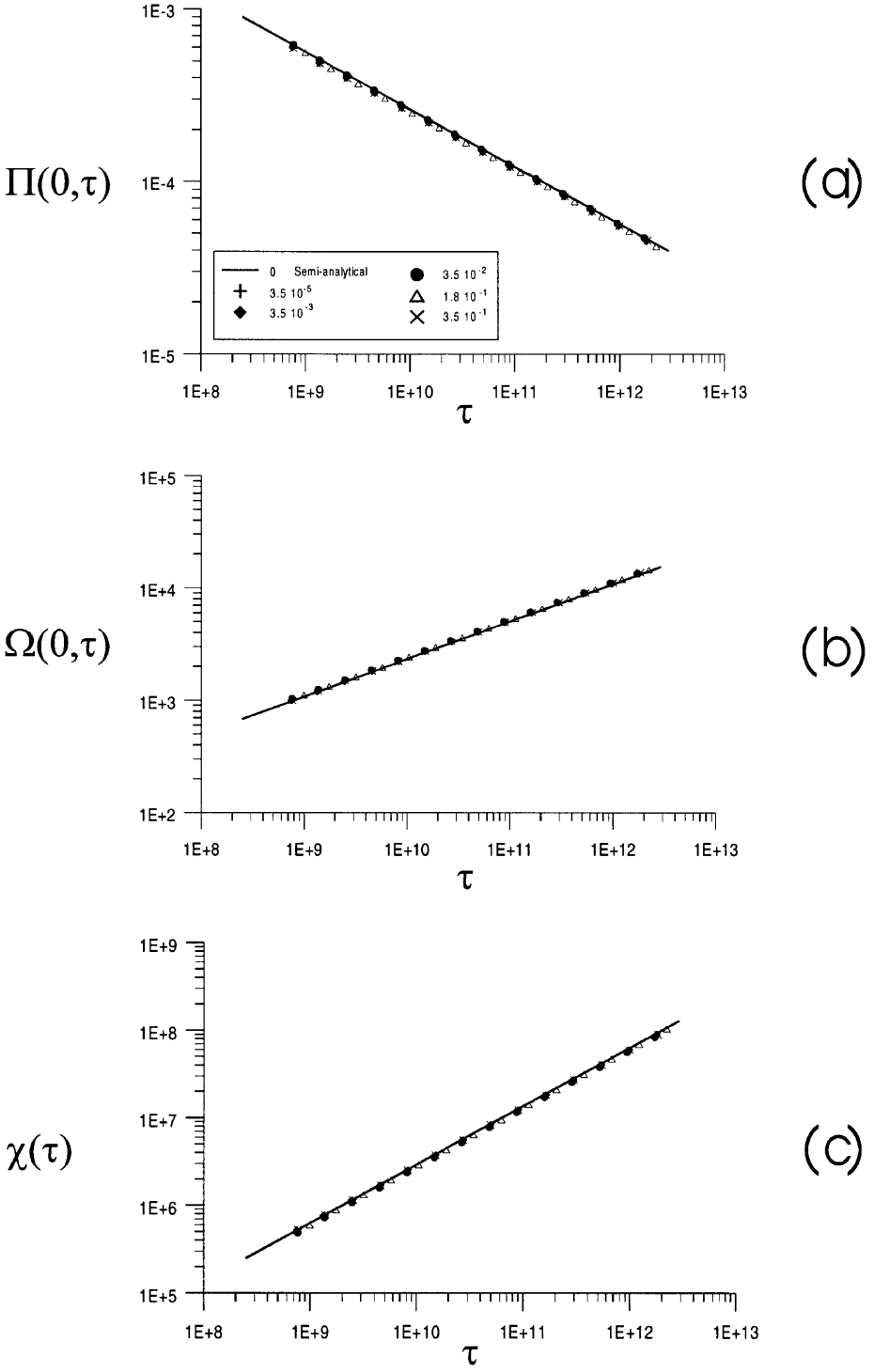

Fig. 2. Solution at the injection point.

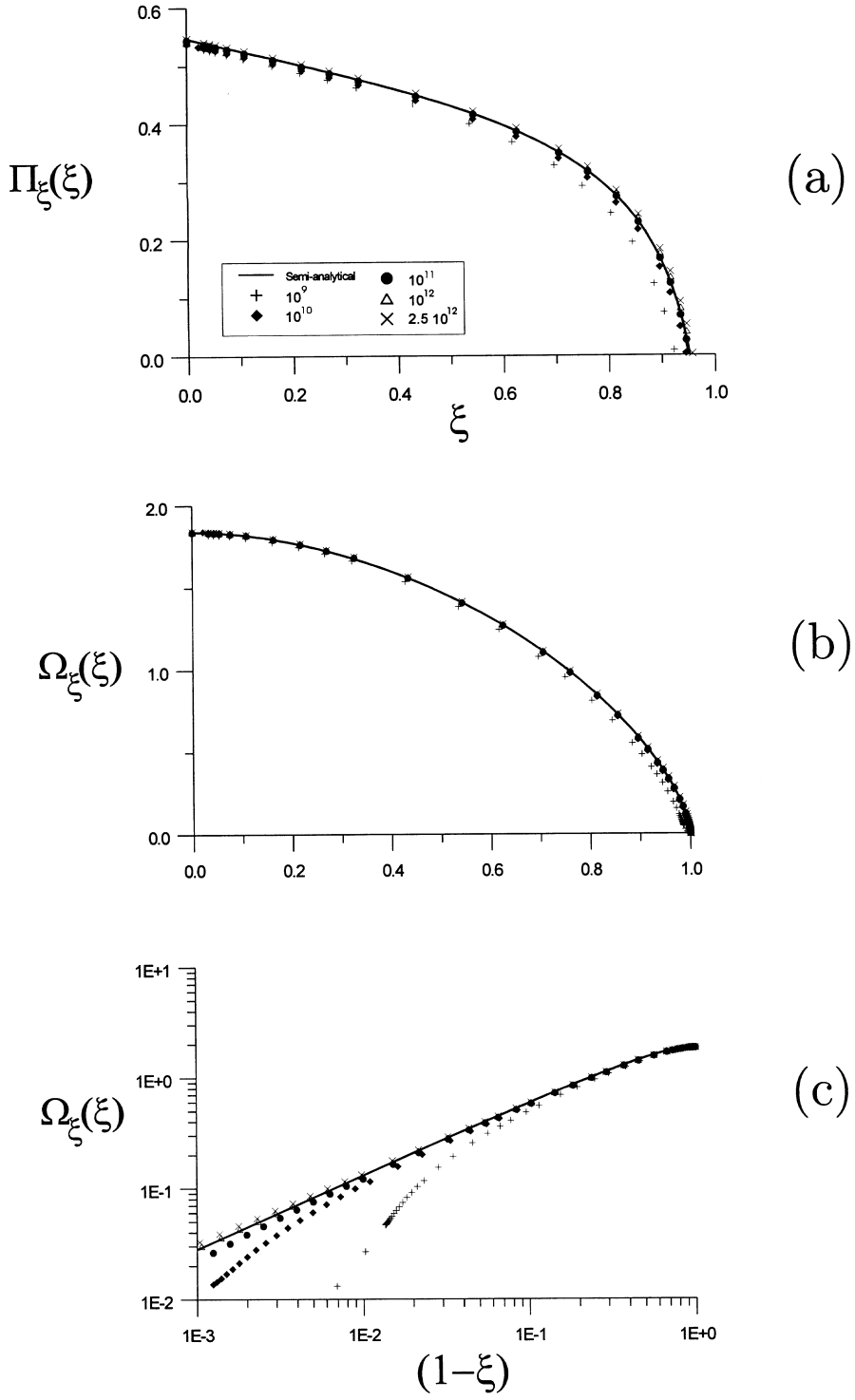

Fig. 3. Net pressure and crack opening profile for the case $\mathscr{K} = 3.5 \times 10^{-5}$.

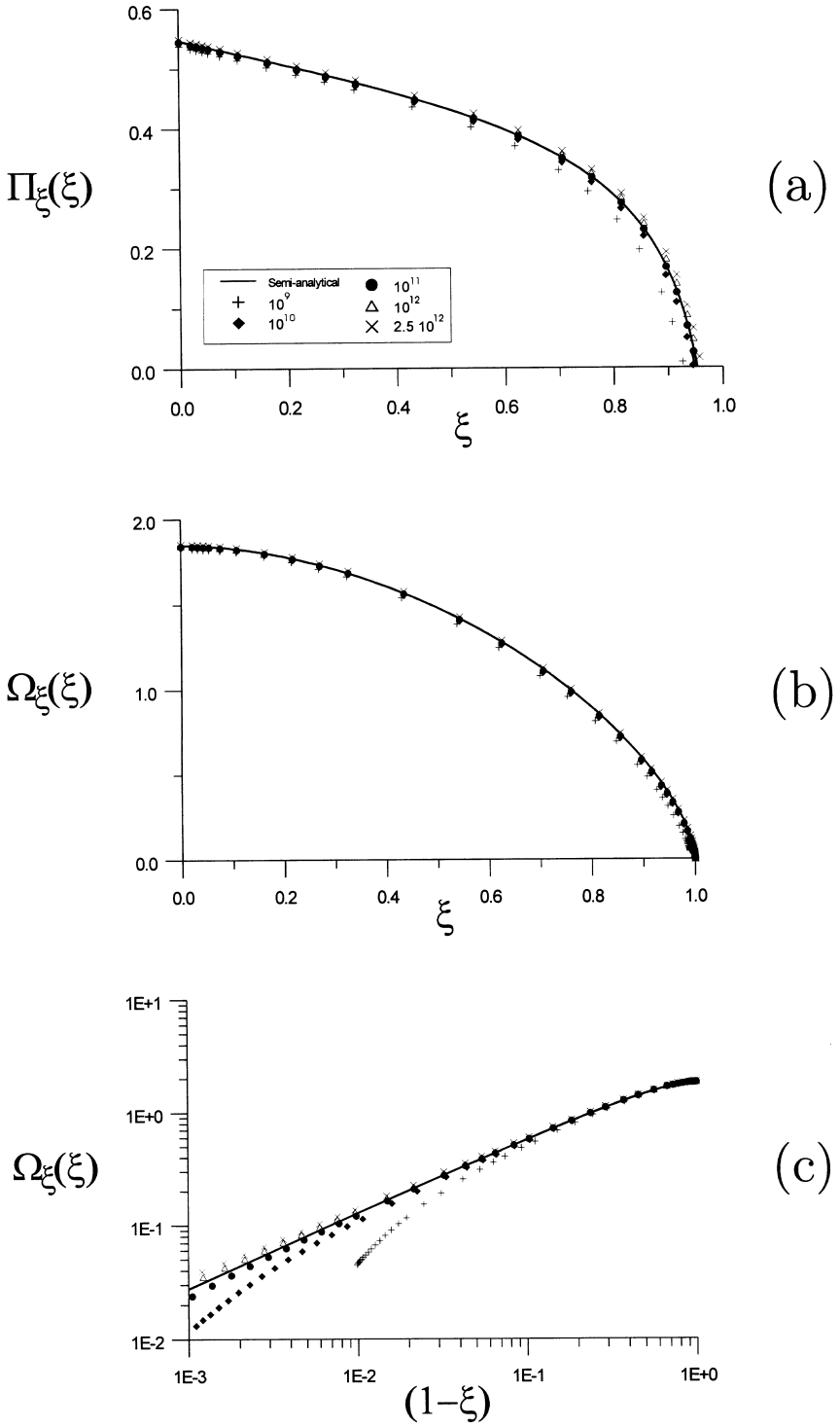

Fig. 4. Net pressure and crack opening profile for the case $\mathscr{K} = 3.5 \times 10^{-2}$.

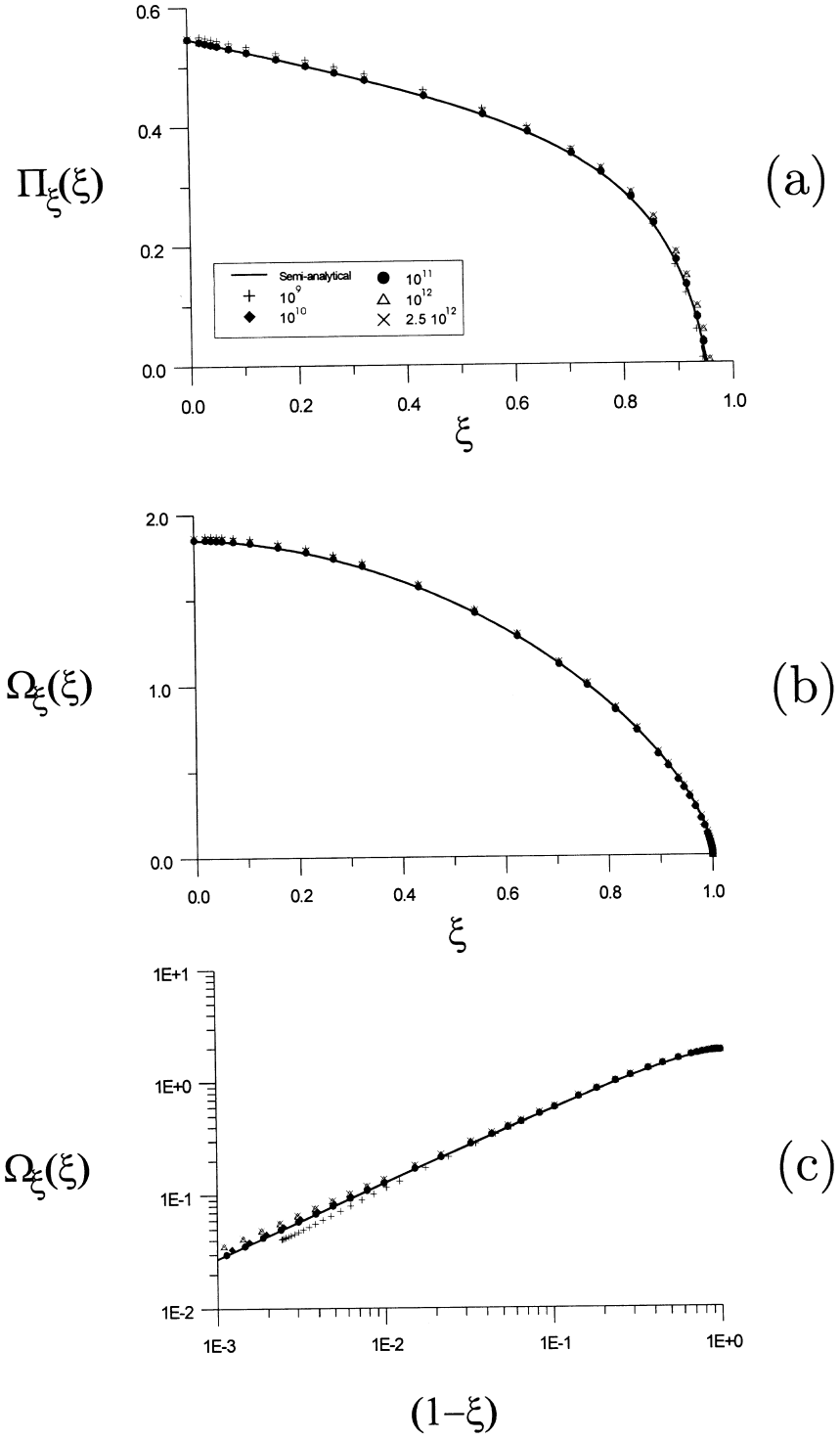

Fig. 5. Net pressure and crack opening profile for the case $\mathscr{K} = 1.7 \times 10^{-1}$.

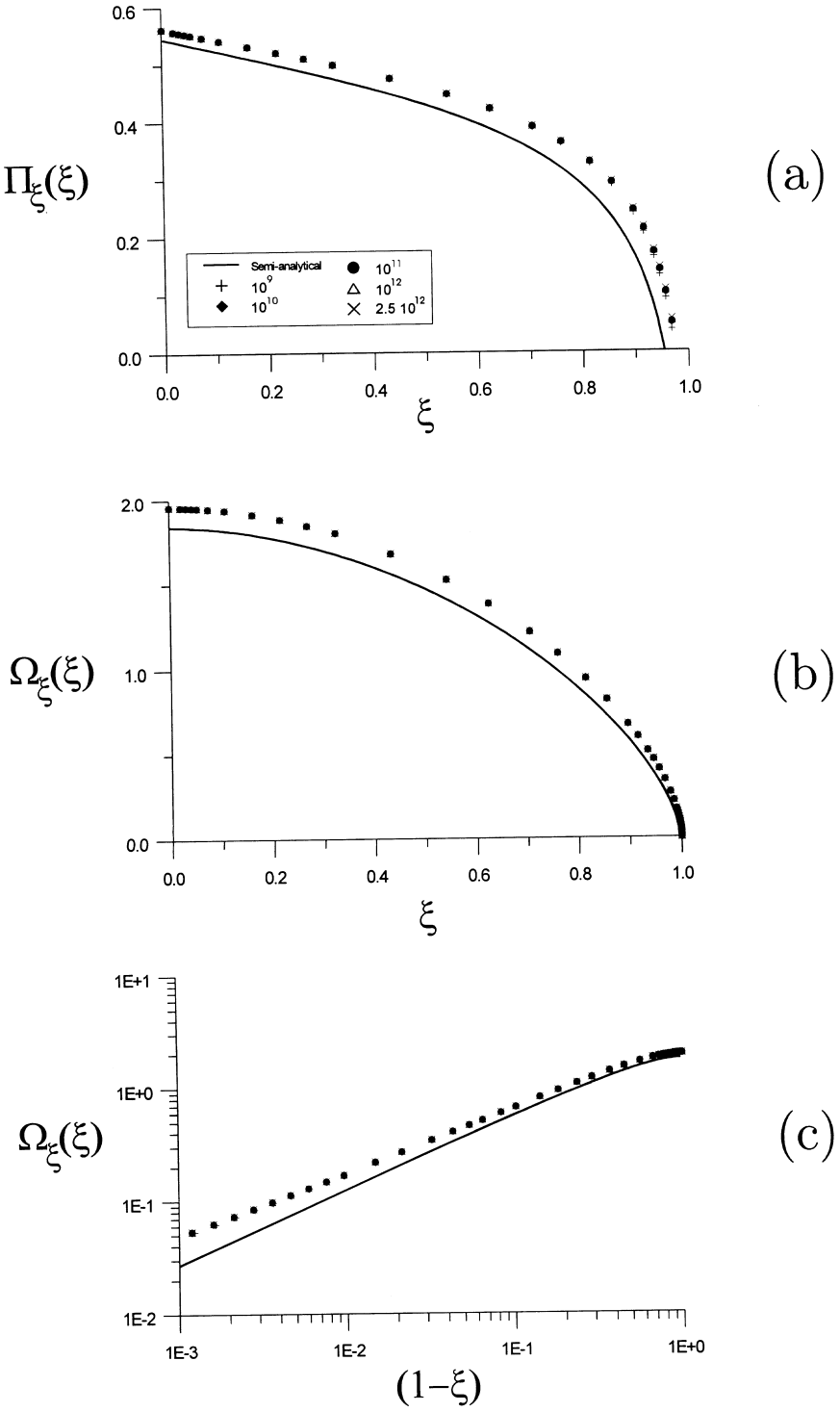

Fig. 6. Net pressure and crack opening profile for the case $\mathscr{K} = 3.5 \times 10^{-1}$.

of simulations carried out for $\mathscr{K} \leqslant 10^{-1}$, suggest that the CD solution, built on the assumptions of zero fluid lag and zero toughness, has some relevance.

4.3. Discussion

To cast these observations into a different perspective, we first observe that the power law dependence on time exhibited by the numerical results imply the same power law dependence on time for both the viscous dissipation $\mathscr{D}$ ($\mathscr{D}$ is actually the dissipation scaled by the characteristic value $\Gamma = E'L^2/T$) and the energy rate $2\mathscr{G}\dot{\lambda}$ expended in creating new fracture surfaces ($\mathscr{G} = \mathscr{K}^2$ denotes the dimensionless energy release rate). Indeed,

$$\mathscr{D} = \delta\tau^{-1/3} \quad \delta = -2\gamma^2 \int_0^1 \Psi_\xi \Pi'_\xi \, \mathrm{d}\xi \tag{24}$$

and

$$2\mathscr{G}\dot{l} = \frac{4}{3}\mathscr{K}^2\gamma\tau^{-1/3}. \tag{25}$$

It is conjectured that the CD solution applies under conditions where the rate of energy dissipated in the solid to extend the fracture energy is small in comparison with the viscous dissipation in the fluid. The condition, under which the CD solution is expected to appropriately describe the behavior of a hydrofracture, can then be stated in terms of a dimensionless number θ which is simply proportional to $\mathscr{K}^2$

$$\theta = \frac{\mathscr{G}\dot{\lambda}}{\mathscr{D}} = \frac{4\gamma\mathscr{K}^2}{3\delta}. \tag{26}$$

Values of δ, γ and θ for the CD solution ($\mathscr{K} = 0$) and the numerical simulations are presented in Table 1.

Thus in more general terms, the results of this study (summarized in Table 1) suggest the existence of three regimes of solution, which could be discriminated in terms of the dissipation ratio θ:

Table 1
Value of γ, δ and θ for different $\mathscr{K}$

$\mathscr{K}$	γ	δ	θ
0	0.613	0.408	0
3.5×10^{-5}	0.616	0.362	2.8×10^{-9}
3.5×10^{-3}	0.613	0.369	2.7×10^{-5}
3.5×10^{-2}	0.615	0.383	2.6×10^{-3}
1.7×10^{-1}	0.609	0.441	5.3×10^{-2}
3.5×10^{-1}	0.580	0.309	3.1×10^{-1}

First line corresponds to the semi-analytical solution.

- $\theta < 10^{-2}$, viscosity-dominated regime for which the CD solution applies;
- $10^{-2} < \theta < 10^{-1}$, transition regime;
- $\theta > 10^{-1}$, toughness-dominated regime.

Additional simulations are needed, however, to ensure the appropriateness of distinguishing uniquely the different regimes of the hydraulic fracturing process by means of the dimensionless ratio θ. Moreover, a detailed set of simulations is required to explore the behavior of the solution in the transition regime.

The conclusion, that the zero-toughness solution is applicable under conditions of 'small' toughness, is also supported by the solution of a semi-infinite hydraulic fracture propagating in an elastic solid with finite toughness (Garagash and Detournay, 1998). The analysis of this semi-infinite fracture shows that the singular zero toughness solution (8) is actually the asymptotic solution at infinity. In other words, at large enough distance from the tip (increasing with toughness), the solution behaves as if the solid had zero toughness and the fluid was reaching the fracture tip. Translated to the case of a finite fracture, this result thus suggests that the details of the tip solution associated with the rock toughness and a fluid lag becomes inconsequential, if eqn (8) can develop as an intermediate asymptotic solution.

5. Concluding remarks

Numerical simulations of a hydraulic fracture propagating in an impermeable rock exhibit global self-similarity, for a constant injection rate. In particular, the predicted power law dependence on time of the net injection pressure and fracture aperture at the injection point, and fracture length is well observed in the numerical results. Furthermore, there is a very good agreement between the self-similar and the numerical solution, under conditions of 'small' toughness.

This agreement suggests that the semi-analytical zero toughness solution is applicable to cases where the rock has a non-zero fracture toughness and a fluid lag develops, provided that the ratio θ of the rate of energy dissipation in the solid over the viscous dissipation in the fluid is less than 10^{-2}. This study also indicates that the existence of a sizeable fluid lag has a negligible effect, up to $5 \sim 10\%$ of the fracture extension, on the injection pressure and crack aperture at the wellbore.

Acknowledgements

The first author would like to thank Intevep for financial support while he was enrolled in the Ph.D. program at the University of Minnesota. The second author wishes to thank Schlumberger for being able to publish this work. The authors would like also to acknowledge the benefits of many valuable discussions with Anthony Pearson.

Appendix A

Numerical solution for the similarity formulation

The numerical solution of the system eqns (17) and (18) begins with the obtention of a suitable representation for Π_ξ and Ω_ξ. Following the procedure described by Carbonell and Detournay (1998), Π_ξ and Ω_ξ are expressed as the sum of a general and a particular source solution

$$\Pi_{\xi}(\xi) = \Pi^{*}(\xi) + B\Pi^{**}(\xi)$$
$$\Omega_{\xi}(\xi) = \Omega^{*}(\xi) + B\Omega^{**}(\xi) \tag{A.1}$$

where B is an as yet undetermined coefficient. Both the particular $[\Pi^{**}(\xi), \Omega^{**}(\xi)]$ and the general solution $[\Pi^{*}(\xi), \Omega^{*}(\xi)]$ satisfy the elasticity eqn (17).

The particular solution, which is not associated with any stress singularity at the tip, is introduced to account for the discontinuity of the pressure gradient at the source

$$\Pi^{**} = 2 - \pi|\xi|$$
$$\Omega^{**} = 4(1-\xi^2)^{1/2} + 2\xi^2 \ln\left|\frac{1-(1-\xi^2)^{1/2}}{1+(1-\xi^2)^{1/2}}\right|. \tag{A.2}$$

The general solution $\Pi^{**}(\xi)$, $\Omega^{**}(\xi)$ is written in the form of an infinite series of base functions $\Pi_i^{*}(\xi)$, $\Omega_i^{*}(\xi)$

$$\Pi^{*}(\xi) = \sum_{i=1}^{\infty} A_i \Pi_i^{*}(\xi)$$
$$\Omega^{*}(\xi) = \sum_{i=1}^{\infty} A_i \Omega_i^{*}(\xi) \tag{A.3}$$

where each base function is expressed in terms of orthogonal Jacobi polynomials as follows

$$\Pi_i^{*} = -\frac{1}{4\times 3^{1/2}}\left\{P_{2i-1}^{(-1/3,1/3)}(\xi)\left[\left(\frac{1+\xi}{1-\xi}\right)^{1/3}+2\right] - P_{2i-1}^{(1/3,-1/3)}(\xi)\left[\left(\frac{1-\xi}{1+\xi}\right)^{1/3}+2\right]\right\} \tag{A.4}$$

$$\Omega_i^{*} = \frac{1}{2(2i-1)}[P_{2i-2}^{(2/3,4/3)}(\xi)(1-\xi)^{2/3}(1+\xi)^{4/3} + P_{2i-2}^{(4/3,2/3)}(\xi)(1+\xi)^{2/3}(1-\xi)^{4/3}]. \tag{A.5}$$

An n-order approximation $\Pi_{\xi}^{(n)}(\xi)$, $\Omega_{\xi}^{(n)}(\xi)$ to $\Pi_{\xi}(\xi)$, $\Omega_{\xi}(\xi)$ is then sought by truncating the series representation of eqn (A.3) after n terms. Substituting $\Pi_{\xi}^{(n)}(\xi)$, $\Omega_{\xi}^{(n)}(\xi)$ into the lubrication eqn (18), leads to the formulation of a non-linear algebraic equation in terms of the $(n+1)$ unknowns $A_i^{(n)}$, $i = 1, n$ and $B^{(n)}$. This equation takes the form

$$\Xi^{l}(\xi, A_i^{(n)}, B^{(n)}) - \Xi^{r}(\xi, A_i^{(n)}, B^{(n)}) = 0 \tag{A.6}$$

where Ξ^{l} and Ξ^{r} are given by

$$\Xi^{l}(\xi, A_i^{(n)}, B^{(n)}) = \sum_{i=1}^{n} A_i^{(n)}\left[I_i^{*}(\xi) + \frac{2}{3}\xi\Omega_i^{*}(\xi)\right] + B^{(n)}\left[I^{**}(\xi) + \frac{2}{3}\xi\Omega^{**}(\xi)\right]$$
$$\Xi^{r}(\xi, A_i^{(n)}, B^{(n)}) = -\left[\sum_{i=1}^{n} A_i^{(n)}\Omega_i^{*}(\xi) + B^{(n)}\Omega^{**}(\xi)\right]^{3}\left[\sum_{i=1}^{n} A_i^{(n)}\Pi_i^{*\prime}(\xi) + B^{(n)}\Pi^{**\prime}(\xi)\right]. \tag{A.7}$$

In the above equations, $I_i^{*}(\xi)$ and $I^{**}(\xi)$ denote two integrals, respectively defined as

$$I_i^*(\xi) = \int_\xi^1 \Omega_i^*(\rho)\,\mathrm{d}\rho \tag{A.8}$$

$$I^{**}(\xi) = \int_\xi^1 \Omega^{**}(\rho)\,\mathrm{d}\rho. \tag{A.9}$$

The integrals $I_i^*(\xi)$ and $i^{**}(\xi)$ can be solved analytically; their close-form expressions are given by Carbonell (1996).

Finally, a non-linear least-squares collocation method is used to solve for the $n+1$ unknown coefficients $A_i^{(n)}$, $i = 1, n$ and $B^{(n)}$. The numerical algorithm consists in seeking the unknown coefficients such that eqn (A.6) is satisfied at each of a set of $n+1$ collocation points ξ_i, $i = 1, n+1$. The coefficients $A_i^{(n)}$, $i = 1, n$ and $B^{(n)}$ are determined by minimizing the objective function $\Delta\,(A_i^{(n)}, B^{(n)})$ defined as

$$\Delta = \sum_{j=1}^{n+1}\left(\frac{\Xi^l(\xi_j, A_i^{(n)}, B^{(n)})}{\Xi^r(\xi_j, A_i^{(n)}, B^{(n)})} - 1\right)^2. \tag{A.10}$$

Note that the solution corresponds not only to the minimum of the least-squares error Δ, but also to the vanishing of Δ.

The minimization is carried out using the steepest descent method. The convergence tests for the minimization are

$$|A_{i,k}^{(n)} - A_{i,k+1}^{(n)}| < \varepsilon \tag{A.11}$$

and

$$\Delta_{k+1}(A_{1,k}^{(n)}, \ldots, A_{n,k}^{(n)}, B_k^{(n)}) = \Delta_{k+1}(A_{1,k+1}^{(n)}, \ldots, A_{n,k+1}^{(n)}, B_{k+1}^{(n)}) \tag{A.12}$$

where the 'equality' in eqn (A.12) has to be understood at the machine precision. In the above, the subscript k characterizes the value of a coefficient at the kth iteration, and ε is an arbitrary small number.

In general, calculations have been done using values of $\varepsilon = 10^{-6}$ for the convergence test, with rapid convergence in $k\text{th} \leqslant 10$ iterations. Numerical calculations have shown that, for any initial guess of coefficients $A_{i,0}^{(n)}$ and $B_0^{(n)}$, to minimize the objective function $\Delta\,(A_i^{(n)}, B^{(n)})$, yields the same minimum point or final set of coefficients. It implies that $\Delta\,(A_i^{(n)}, B^{(n)})$ has a well-defined minimum.

Appendix B

Numerical model (*Loramec*)

Preamble

Loramec is a numerical model for the propagation and closure of hydraulic fractures of simple radial and plane strain geometries (Desroches and Thiercelin, 1993; Desroches, 1998). We detail here only the hypotheses and implementation related to the propagation of a plane strain fracture driven by a Newtonian fluid in an impermeable medium.

The physical processes modelled by Loramec include the opening of the fracture through fluid pressure, the creation of new fracture surface, the motion of the fluid in the fracture and the percolation of the fluid into the solid through the fracture walls (which is neglected here). The following assumptions are made: the fractured material is infinite, isotropic and linear elastic; the fracture is considered as a surface of discontinuity in the elastic medium across which there is a jump in normal displacement corresponding to the aperture of the fracture; the fracture is planar and propagates perpendicularly to the minimum principal stress direction; the fracture propagation is quasi-static; the fracturing fluid is incompressible and its rheological behavior is Newtonian; the fluid does not necessarily reach the tip of the fracture: there is a possibility of a dry zone, or fluid lag, at the fracture tip.

The solution of the model consists of, at any time after fluid injection has started, the extension of the fracture, the position of the fluid front, the distribution of fluid pressure and fracture width along the fracture extension.

Formulation

The algorithm is based on an integro-variational approach for the elasticity equation, relating the gradient of the fracture aperture to the net pressure of the fluid in the fracture (Nedelec, 1980). It is obtained through a variational formulation on the elasticity equation written as an integral equation. Like in a classical boundary value problem, the reduction of the problem to the dimension of the fracture surface is conserved. The singularity of the kernel is reduced to a Cauchy singularity. Finally, provided that the Mode I stress intensity factor K_I is strictly positive, this formulation ensures the correct behavior of the fracture width in the vicinity of the tip of the fracture without resorting to special elements.

Taking into account the symmetry of the problem, the integro-variational formulation of the elasticity equation for that particular geometry is

$$\frac{E'}{4\pi}\int_0^l\int_0^l \ln\left|\frac{x+x'}{x-x'}\right|\frac{\partial w}{\partial x}\frac{\partial \hat{w}}{\partial x'}\,dx\,dx' = \int_0^l p(x')\hat{w}(x')\,dx' \tag{B.1}$$

where $\hat{w}$ is a virtual fracture opening field.

The lubrication eqn (2) is multiplied by a space weighting function and integrated over the wet length of the fracture. Following the work by Bonnerot and Jamet (1974, 1979) on Stefan problems, the resulting equation is multiplied by a weighting function depending on time only and integrated on the time step. Although this operation results into a much more complex formulation, it also yields great stability to the solution.

The creation of new fracture surface is taken into account by computing the mode I stress intensity factor K_I. The stress intensity factor is computed using the Bueckner–Rice (Bueckner, 1970; Rice, 1972) weight function; for the symmetric plane strain fracture of concern, K_I can be expressed as:

$$K_I = 2\sqrt{\frac{l}{\pi}}\int_0^l \frac{p(x)}{\sqrt{l^2-x^2}}\,dx. \tag{B.2}$$

The following set of initial/boundary conditions, including the propagation criterion, is also considered.

- The far-field minimum principal stress σ_o is assumed to be known and constant in space and time. The constant rate of fluid injection into the fracture, Q_o, is also given.
- The aperture of the fracture at the tip is zero.
- If there is a dry zone (between the fracture tip and the fluid front), the pressure in this zone is set to either the far-field formation pressure for high permeability rocks, or as the fracturing fluid vapor pressure for low permeability rocks.
- If the computed size of the dry zone is zero, the fluid pressure at the tip is a priori unknown and is computed as part of the solution.
- If the fracture is propagating, the mode I stress intensity factor K_I is equal to the fracture toughness of the material K_{Ic}, and the speed of the fluid at the fluid front is equal to the speed at which the fluid front itself moves (Stefan boundary condition).

Implementation considerations

Two sets of independent variables are considered for the description of space and time. The first set consists of (x, t) where x is the distance measured from the center of the wellbore along one wing of the fracture and t is the time with its origin taken at the start of fluid injection. The second set consists of normalized quantities better suited to the adopted discretization strategy: (ξ', τ), where ξ' is a normalized distance equal to 0 at the wellbore radius and 1 at the fluid front of the fracture, and τ is a normalized time equal to 0 at instant t_n and 1 at instant t_{n+1}.

The width and the fluid pressure are discretized in the stretching space ξ' and in time t. A stretching mesh with a constant number of isoparametric elements is used. This approach has numerous advantages: it avoids the need for adding or collapsing elements in the course of the simulation. Also, each element in the wet zone of the fracture keeps a constant position in the normalized system of coordinates (ξ', τ). The numerical coefficients needed to evaluate integrals over a particular element need therefore to be computed only once, resulting in significant speed up of the computation.

The equations mentioned above are mapped from the (x, t) to the (ξ', τ) system of variables. A Galerkin formulation is then used for both the elasticity and the fluid flow equation, together with a linear interpolation in time and a quadratic interpolation in ξ'.

Given the complete solution at time t_n, the solution scheme consists of three loops. In the lowest level loop, the fluid flow and the elasticity equations are solved concurrently for nodal width and pressure with a Newton–Raphson scheme. In the intermediate level loop, the propagation criterion is checked, and the tip boundary condition modified accordingly: either the size of the fluid lag is changed, or the pressure at the tip is changed if the size of the lag is zero. In the top level loop, the global mass balance is checked and the time step modified accordingly.

Once the final solution for a particular time step is found, it is recorded and the fracture is advanced by a fraction of its length (between 1 and 5%, usually about 2%) and the solution scheme started again.

Note that the algorithm presented above is working on the basis that the complete solution is known at the previous time stage. This raises the problem of finding the solution for the first considered time stage t_1. In fact, as noted in this paper, the behavior of the width and pressure profiles exhibits self-similarity for a constant injection rate. This self-similarity is used for this first time stage to obtain a formulation depending on $w(t_1)$ and $p_f(t_1)$ only. Once the first solution is obtained, the solution scheme switches to the two points recurrence scheme described previously.

References

Batchelor, G.K., 1967. An Introduction to Fluid Mechanics. Cambridge University Press.
Bonnerot, R., Jamet, P., 1974. A second order finite element method for the One-Dimensional Stefan problem. Int. J. Numer. Meth. Engng. 8, 811–820.
Bonnerot, R., Jamet, P., 1979. A third order accurate discontinuous finite element method for the one-dimensional Stefan problem. J. Comp. Phys. 32 (2), 145–167.
Bueckner, H.F., 1970. A novel principle for the computation of stress intensity factors 50 (9), 529–546.
Carbonell, R.S., 1996. Self-similar solution of a fluid-driven fracture. Ph.D. thesis, University of Minnesota.
Carbonell, R.S., Detournay, E., 1998. Self-similar solution of a fluid driven fracture in a zero toughness elastic solid. Proc. Roy. Soc. London, Ser. A submitted for publication.
Desroches, J., 1998. Modeling propagation and closure of hydraulic fractures of simple geometries. Int. J. Numer. Anal. Methods Geomech., in preparation.
Desroches, J., Thiercelin, M., 1993. Modeling propagation and closure of micro-hydraulic fractures. Int. J. Rock Mech. Min. Sci. Geomech. Abstr. 30, 1231–1234.
Desroches, J., Detournay, E., Lenoach, B., Papanastasiou, P., Pearson, J.R.A., Thiercelin, M., Cheng, A.H.-D., 1994. The crack tip region in hydraulic fracturing. Proc. Roy. Soc. London, Ser. A A447, 39–48.
Garagash, D., Detournay, E., 1998. Similarity solution of a semi-infinite fluid-driven fracture in a linear elastic solid. C. R. Acad. Sc. Paris, t. 326, Série IIb, pp. 285–292.
Geertsma, J., Haafkens, R., 1979. A comparison of the theories for predicting width and extent of vertical hydraulically induced fractures. ASME J. Energy Res. Tech. 101, 8–19.
Nedelec, J.C., 1980. Formulations variationelles de quelques equations integrales faisant intervenir des parties finies. Proceedings of the Second International Symposium on Innovative Numerical Analysis, Montreal, Canada.
Nilson, R.H., 1988. Similarity solutions for wedge-shaped hydraulic fracture driven into a permeable medium by a constant inlet pressure. Int. J. Numer. Anal. Methods Geomech. 12, 477–495.
Nordgren, R.P., 1972. Propagation of vertical hydraulic fracture. Soc. Pet. Eng. J., Trans. AIME 253, 306–314.
Perkins, T.K., Kern, L.R., 1961. Widths of hydraulic fractures. J. Pet. Tech., Trans. AIME 222, 937–949.
Rice, J.R., 1968. Mathematical Analysis in the Mechanics of Fracture, vol. II of Fracture, an Advanced Treatise. Academic Press, Chapter 3, pp. 191–311.
Rice, J.R., 1972. Some remarks on elastic crack-tip stress fields. Int. J. Solids Structures 8 (6), 751–758.
Spence, D.A., Sharp, P, 1985. Self-similar solution for elastohydrodynamic cavity flow. Proc. Roy. Soc. London, Ser. A A400, 289–313.